Lasers in Manufacturing Conference 2019

Reflective pump-probe microscopy of ultrashort laser pulses: Energy deposition of burst pulses in alkali aluminosilicate glass

Martin Kratz[a*], Christian Kalupka[b], Franca auf der Heiden[b], Stefan Quach[b]

[a]*Chair for Laser Technology LLT, RWTH Aachen University, Steinbachstraße 15, 52074 Aachen, Germany*
[b]*Fraunhofer Institute for Laser Technology ILT, Steinbachstraße 15, 52074 Aachen, Germany*

Abstract

The application of ultrashort laser pulses for processing of wide bandgap materials like glasses is a promising approach in the glass and semi-conductor industry. Burst pulses have been identified as a key parameter for improving processes like glass-cutting, surface structuring or involume modification. Undesired damages in the modification region leading to mechanical stresses, chipping and crack formation are challenging problems. To generate a deeper insight of damage mechanisms, we investigate the energy deposition using bursts of ultrashort laser pulses in alkali aluminosilicate glass. The electronic excitation and energy deposition is analyzed in situ during the first 24 ps after illumination by ultrafast pump-probe microscopy. With an advanced experimental setup, we are able to vary the pulse energy and the temporal shift between subsequent pulses in a burst train of two pulses. The results of burst pulse processing are compared to single pulse processing to expose different energy deposition due to the temporal proximity of bursts.

Keywords: ultrashort pulsed laser; pump-probe microscopy; non-linear absorption; microfabrication of glass; burst processing;

1. Introduction

Ultrashort pulsed (USP) laser radiation for processing of transparent dielectrica is used for multiple applications like glass cutting with elongated beam profiles (Mishchik, 2017; Kumkar, 2018; Jenne, 2018; Flamm, 2019), front and rear side drilling of thin holes (Grossmann, 2017; Kumkar, 2018), selective laser induced etching (Hermans, 2014). High intensities in the order of 10^{12} W/cm^2 to 10^{14} W/cm^2 lead to non-

* Corresponding author. Tel.: +49-241-8906-581; fax: +49-241-8906-121.
E-mail address: martin.kratz@llt.rwth-aachen.de.

linear absorption effects and therefore yield an energy deposition into the transparent dielectric (Vogel, 2005; Sun, 2017; Kalupka, 2017).

The utilization of bursts leads to advantageous results for many processes like for example deeper holes in drilling applications or a more localized plasma generation which generates cracks for high-quality glass cutting with elongated beams (Esser, 2011; Mishchik, 2017; Kumkar, 2018; Jenne, 2018; Flamm, 2019). The difference in the results after applying bursts may be attributed to a changed energy deposition of the subsequent pulses after the first pulse in one burst. Therefore, the material has to be excited temporarily to a more favorable state for energy coupling between photons and electrons by the previous pulse. Studies state that this effect leads to accumulative processes which yield these mentioned advantageous results for drilling and glass cutting (Esser, 2011; Bergner, 2018). Several studies investigate this phenomenology in situ (Hendricks, 2016; Kumkar, 2018; Jenne, 2019). The mechanism for the more favorable energy deposition of subsequent pulses in a burst train is still under debate.

In this study we investigate the energy deposition of the second pulse with a time shift of $\Delta T = 13.8\ \mathrm{ns}$ to the first pulse in a burst train into transparent dielectrics. Especially, the hypothesis of higher energy deposition is examined ex situ by topology measurements with a laser scanning microscope and in situ by time-resolved pump-probe microscopy with a reflective setup. The pump beam is focused on the surface of alkali aluminosilicate glass. Two pump pulses are generated with a Michelson interferometer. To attribute effects to the temporal shift between the pulses, all experiments are conducted in three pulse sequence configurations. The configurations are single pulse, double pulses with several seconds time shift ($\Delta T \to \infty$) and double pulses with a $\Delta T = 13.8\ \mathrm{ns}$ time shift.

In section 3 the experimental results for the three pulse sequence configurations are presented. The ex situ measurements of the ablation geometry (section 3.1) and the in situ pump-probe measurements with a time delay between pump and probe pulse up to $24\ \mathrm{ps}$ after the last pulse (section 3.2) are discussed.

2. Experimental Setup

The experimental pump-probe setup is displayed in Fig. 1. A Ti:sapphire chirped pulse amplification laser system (Coherent Libra) with a central wavelength of $800\ \mathrm{nm}$, a minimum pulse duration of $100\ \mathrm{fs}$ (FWHM) and a maximum pulse energy of $2\ \mathrm{mJ}$ is used to trigger single pulse events. The minimum pulse duration is utilized during the experiments. The pulse is split into a pump and a probe pulse. The probe pulse is frequency converted by a Beta Barium Borat crystal to a wavelength of $400\ \mathrm{nm}$. It can be shifted temporally by a delay line in a range from 0 to $30\ \mathrm{ns}$. For imaging, the probe pulse is focused in the backside focal plane of a microscope objective ($20\mathrm{x}$, $NA = 0.40$, $WD = 12.0\ \mathrm{mm}$) to illuminate the sample homogeneously. A polarizing beam splitter in combination with a quarter wave plate is placed between the focusing lens and the microscope objective. The reflected light takes the path from the sample through the microscope objective on the CMOS camera. A band pass filter with a central wavelength of $400\ \mathrm{nm}$ reduces the illumination to the light of the probe pulse. The pump pulse energy is regulated by a half wave plate in combination with a polarizing beam splitter. Then the pump pulse is divided temporally with a Michelson interferometer. A polarizing beam splitter cube is utilized. A half wave plate is placed in front of the polarizing beam splitter cube to adjust the ratio of the pulse energies of the two generated pump pulses. The transmitted pulse is reflected back to the beam splitter cube. Thereby, it passes a quarter wave plate twice and the polarization is rotated by $90°$. The reflected pulse is temporally shifted by a delay line, redirected by a retroreflector and reflected back by a mirror in combination with a quarter wave plate to rotate the polarization by $90°$. The delay line of the pump pulse is utilized to adjust the time shift between the two split pump pulses. After passing the Michelson interferometer both pulses have orthogonal linear polarization due to the polarizing beam splitter cube. The pump pulses are lead to the pump-probe setup and focused

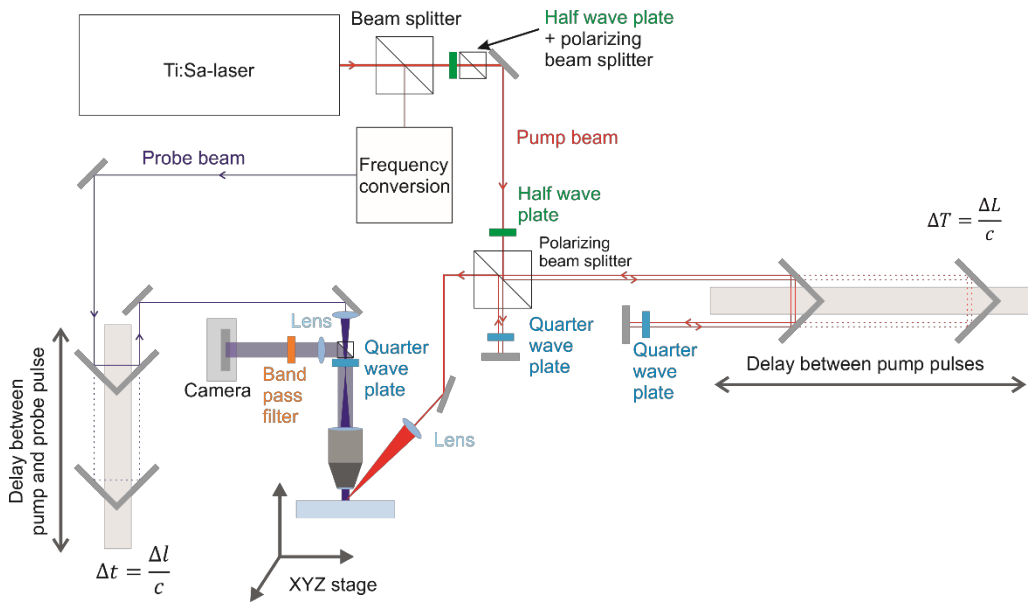

Fig. 1. Schematic view of the pump-probe setup for time-resolved reflectivity measurements.

with a plano-convex focusing lens ($f = 150$ mm) under an angle of $42.5°$ to the normal on the glass surface. All experiments which are presented here are obtained under these focus conditions.

For each measured event two images are recorded. The background is recorded with a blocked pump pulse to get an image of the undamaged surface. The second image is recorded during or after the pump pulse reaches the glass surface. The corresponding pixels of both images are divided to obtain an image of the relative reflectivity R_{rel}. By this way all images are normalized. Selected modifications have been analyzed with a laser scanning microscope (Keyence LSM VK-9700) to get topological information.

3. Results and Discussion

For the three pulse sequence configurations ex situ topology measurements and in situ time-resolved pump-probe microscopy measurements are performed for three different pulse energies. The topology measurements are presented in section 3.1 to substantiate the pump-probe microscopy measurements with respect to the coherence between ablation and electronic excitation. The pump-probe microscopy measurements are performed to get the time evolution of the plasma during the first 24 ps after illumination. The results are discussed in section 3.2.

3.1. Ex situ measurements of modification topology

The depth and the width of the ablated modifications on the glass surface are investigated for three different pulse energies of 18 µJ, 45 µJ and 72 µJ. The ablation width corresponds to the semi-major axis of the elliptical modification. The stated energies refer to the energy of a single pulse measured at the sample position. The experiments are conducted with double pulses separated by a time shift of $\Delta T \to \infty$ and $\Delta T = 13.8$ ns. The results are depicted in Fig. 2. The standard deviation is determined by 3 measured values per parameter.

The ablation depth increases with pulse energy for both configurations (Fig. 2a). For a pulse energy of $E_{\mathrm{Pulse}} = 18$ µJ the ablation depth of the pulse configuration with $\Delta T = 13.8$ ns is 0.22 µm and with $\Delta T \to \infty$ it is 0.24 µm. Both values are consistent within their standard deviation. For 45 µJ and 72 µJ the ablation depth values for double pulse modification with $\Delta T \to \infty$ and $\Delta T = 13.8$ ns differ significantly. The ablation depth for $\Delta T = 13.8$ ns (with 0.34 µm for $E_{\mathrm{Pulse}} = 45$ µJ and 0.36 µm for $E_{\mathrm{Pulse}} = 72$ µJ) is smaller than the ablation depth for $\Delta T \to \infty$ (with 0.45 µm for $E_{\mathrm{Pulse}} = 45$ µJ and 0.50 µm for $E_{\mathrm{Pulse}} = 72$ µJ). A higher energy deposition from the pulse into the glass is attributed to a deeper ablation. Therefore, the experiments reveal a lower energy deposition of the second pulse with a time shift of $\Delta T = 13.8$ ns compared to the second pulse$\Delta T \to \infty$. Thereby, it is assumed that the first pulse of both double pulse sequence configurations yields the same ablation result since it is not influenced by any previous pulse.

The ablation diameter which is denoted as ablation width does not differ significantly for higher pulse energies (Fig. 2b). It is 30.9 µm for pulses with $\Delta T = 13.8$ ns and 31.5 µm for pulses with $\Delta T \to \infty$ at $E_{\mathrm{Pulse}} = 45$ µJ and 33.5 µm for pulses with $\Delta T = 13.8$ ns and 34.1 µm for pulses with $\Delta T \to \infty$ at $E_{\mathrm{Pulse}} = 72$ µJ. The width for $\Delta T = 13.8$ ns is 18.5 µm for the lower pulse energy of 18 µJ which is close to the ablation threshold. The width for the same pulse energy for $\Delta T \to \infty$ is 13.7 µm. Thus, it is significantly lower than for double pulses with $\Delta T = 13.8$ ns. This indicates that the first pulse excites the illuminated material temporally by decreasing the laser intensity threshold for ablation. For higher pulse energies this effect might vanish since the intensity flanks are much steeper and the additional ablation width cannot be resolved.

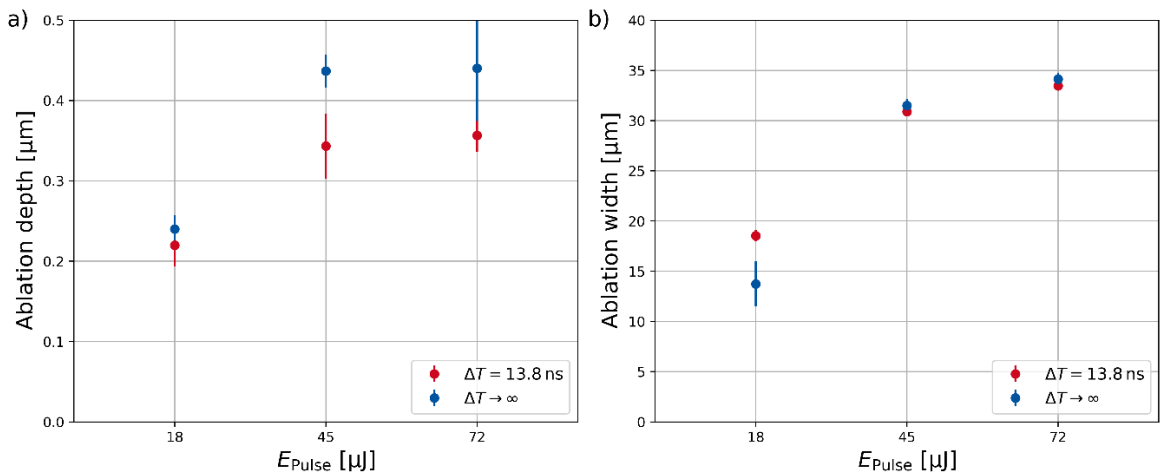

Fig. 1. Measured ablation depth (a) and ablation width (b) for pulse energies of 18 µJ, 45 µJ and 72 µJ and time shifts of $\Delta T = 13.8$ ns and $\Delta T \to \infty$.

3.2. Reflection measurements in temporal vicinity of plasma generation

The relative reflectivity after the second pump pulse with $\Delta T = 13.8$ ns reaches the glass surface is measured to obtain information about the electronic excitation. The results for the probe pulse time delays between 0 and 24 ps are depicted in Fig. 3. The pulse energy is $E_{\mathrm{Pulse}} = 45$ µJ. The time $t = 0.0$ ps denotes the moment when the second pump pulse reaches the sample. At this time two circular, dark zones in the modification are formed by the first pump pulse. The elliptic geometry of the modification is caused by the fact that the pump pulse is focused onto the sample under an angle of $42.5°$ to the normal on the glass surface. The inner and outer edges are clearly visible. The outer edge is the modification edge. Between the outer and inner edge the mean value of the brightest 100 pixels of the relative reflectivity is $R_{\mathrm{rel}} = 1.4 \pm 0.2$. Particles which are ablated by the previous pulse cause inhomogeneities in the relative reflectivity (visible as pixel-sized fluctuations in the brightness). Therefore, the mean value of the 100 brightest pixels is chosen to represent the mean relative reflectivity in this area. The inner contour is not visible at the permanent modification. The mean value for the inner area is $R_{\mathrm{rel}} = 0.9 \pm 0.1$. The inner area remains constantly dark for all pictures up to $t = 23.3$ ps. The relative reflectivity between the inner and outer edge increases for times $t \leq 8.7$ ps. At $t = 8.7$ ps the mean of the brightest 100 pixels of this area is $R_{\mathrm{rel}} = 3.5 \pm 0.3$. In the further course of time the relative reflectivity in this area decreases. After $t = 19.3$ ps the two zones are indistinguishable on the images. Furthermore, the reflectivity outside the excitation zone of the first pulse is increased in vicinity to the outer edge for all images. This indicates the generation of an

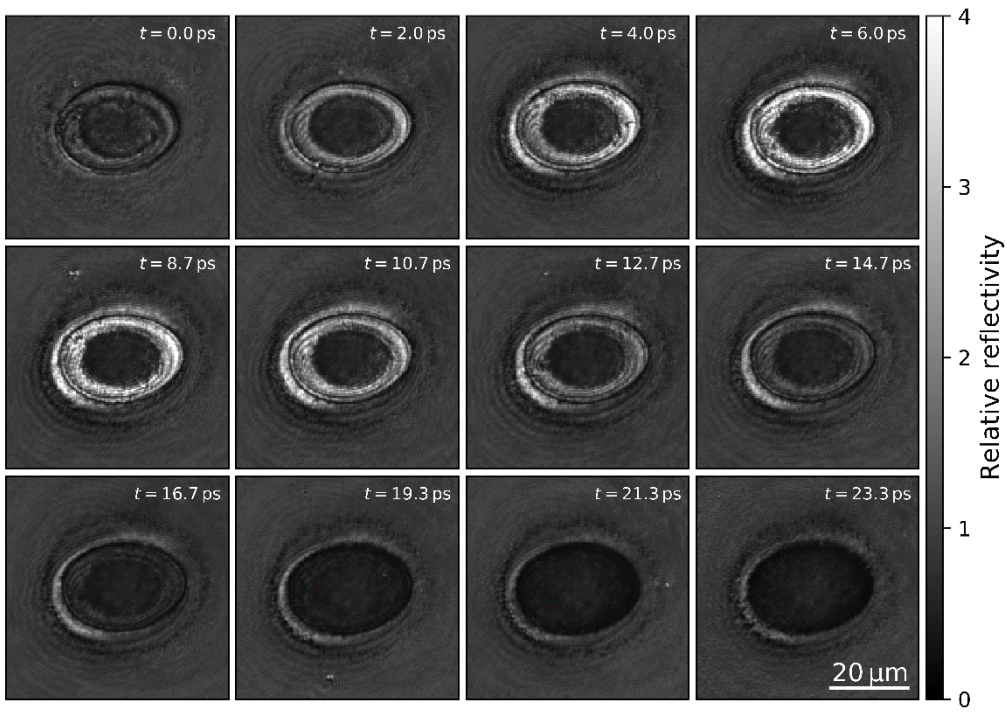

Fig. 2. Time resolved relative reflectivity measurements for double pulses of $\mathrm{E_{Pulse}} = 45$ µJ (single pulse energy) and $\Delta \mathrm{T} = 13.8$ ns from $\mathrm{t} = 0.0$ ps to $\mathrm{t} = 23.3$ ps with respect to the second pulse.

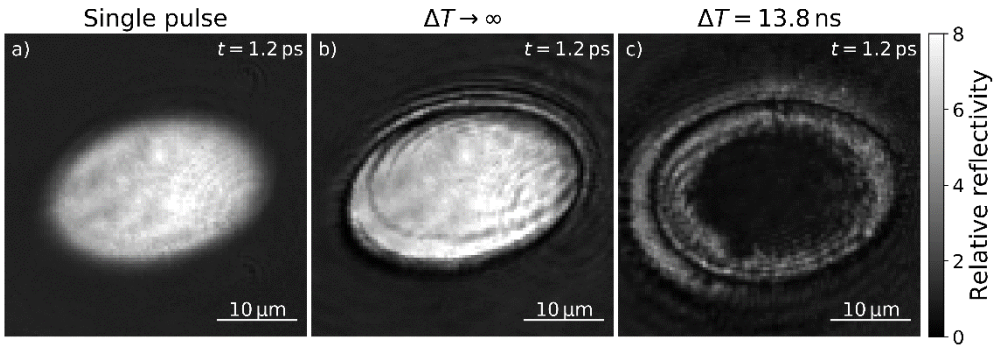

Fig. 3. Time resolved relative reflectivity measurements for a single pulse (a), double pulses with $\Delta T \rightarrow \infty$ (b) and double pulses with $\Delta T = 13.8$ ns (c) at $t = 1.2$ ps after the last pulse incident pulse with single pulse energy of $E_{Pulse} = 45$ µJ.

increased free electron-density outside the modification area of the first pump pulse. The increase of the relative reflectivity occurs after the end of the second pump pulse. Therefore, the free electron-density remains at a high level for about ten to hundred times of the pulse duration time. This behavior has been reported for quartz (Hernandez-Rueda, 2012) and is also in agreement with recent simulation results (Sun, 2017).

To compare the in situ reflectivity results of the three mentioned pulse sequence configurations the pump-probe image for a delay time of $t = 1.2$ ps is depicted in Fig. 4. The delay refers to the last incoming pump pulse of the configuration. The pulse energy is $E_{\mathrm{Pulse}} = 45$ µJ. For a single pulse (Fig. 4a) an elliptic reflectivity zone is obtained whose intensity is decreasing homogeneously from the mid to the outside. The obtained reflectivity after the second pump pulse with $\Delta T \rightarrow \infty$ also exhibits (Fig. 4b) a homogeneously decreasing behavior from the inside to the outside. The values for the relative reflectivity in this area are similar to those of the single pulse. Additionally, the area of high relative reflectivity for the mentioned double pulse configuration is enclosed by a sharp dark edge. Reflectivity images after a delay of $t = 1$ s but before the second pump pulse proved that it is the modification edge from the previous pump pulse. Dark rings and subrings are visible in vicinity to the edge. This effect is attributed to diffraction at the ablation crater of the previous pump pulse. Other explanations like Newton rings which were also observed by single pulse irradiation on glass during reflective pump-probe microscopy measurements (Garcia-Lechuga; 2014) are a possible explanation. Albeit these Newton rings were observed at later delay times of several hundred picoseconds, but only for single pulses. The change of refractive index in the ablation volume is stated to cause these Newton rings. Therefore, further investigations are necessary to check whether such an ablation volume is present after 1.2 ps after the second pump pulse. A different result for the relative reflectivity is obtained at $t = 1.2$ ps after the second pump pulse with $\Delta T = 13.8$ ns (Fig. 4c). As
already mentioned before, a dark area in the center of the modification, lower relative reflectivity values, a larger reflective area and rings at the edges are obtained. The most striking feature in comparison to the double pulse configuration with $\Delta T \rightarrow \infty$ is the dark area in the center. We suggest that it is correlated to the temporal proximity of the pulses of $\Delta T = 13.8$ ns. In combination with the lower ablation depth from section 3.1 this is attributed to a shielding effect by the ablated material from the previous pulse. After 13.8 ns the ablated material from the previous pulse remains slowly moving at a certain height over the focus region and reflects and absorbs the second incoming pump pulse. Therefore, the intensity at the glass surface is lowered significantly, less energy is absorbed and less material is ablated. This is in agreement with

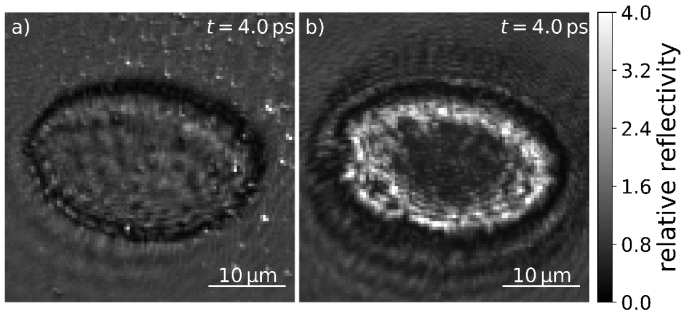

Fig. 4. Time resolved relative reflectivity measurements for double pulse irradiation with a $E_{Pulse,1} = 45$ µJ to $E_{Pulse,2} = 18$ µJ pulse energy ratio for $\Delta T \rightarrow \infty$ (a) and $\Delta T = 13.8$ ns (b) at $t = 4.0$ ps after the second incident pulse.

the ablation depth measurement. A shielding of the probe pulse which incides perpendicular to the glass surface is also assumed. Since the photons from the pump pulse do not transfer momentum significantly the ablated material moves perpendicular to the surface on average. Therefore, the dark area is caused by the shielding of the probe pulse. Nevertheless, the appearance of Newton Rings has to be checked for $\Delta T = 13.8$ ns. The obtained increased reflectivity outside the modification area of the previous pump pulse can be understood as a temporal excitation of the material which lowers the threshold for seeding a free electron-density even though the topology in this area is not changed. The results for the ablation width from section 3.1 support this assumption. For the pulse energy of $E_{\mathrm{Pulse}} = 18$ µJ which is near to the ablation threshold this effect is observable ex situ in the ablation width measurements.

To substantiate these results measurements with double pulses of two different pulse energies per pulse are performed. A first pulse with a pulse energy of $E_{\mathrm{Pulse}} = 45$ µJ and a second pulse with $E_{\mathrm{Pulse}} = 18$ µJ are utilized with a time shift of $\Delta T \rightarrow \infty$ and with $\Delta T = 13.8$ ns. The pulse energy of $E_{\mathrm{Pulse}} = 18$ µJ is close to the ablation threshold for single pulses. A representative relative reflectivity measurement for each configuration is depicted in Fig. 5. The delay between second pump and probe pulse is $t = 4.0$ ps. The relative reflectivity for the pulse configuration with $\Delta T \rightarrow \infty$ (Fig. 5a) shows a slight increase in the top right in the modification regime of the previous pulse. The other regions within this area are unaffected. At least, there is no increased relative reflectivity. The corresponding relative reflectivity measurement for the pulse configuration with $\Delta T = 13.8$ ns (Fig. 5b) exhibits a bright ring around a dark area in the center comparable to the results mentioned above. The regime of high reflectivity does not reach the modification edge of the previous 45 µJ-pulse. This is attributed to the smaller diameter of the focus area which has an intensity above the ablation threshold. The most striking result is that the temporal proximity of $\Delta T = 13.8$ ns from the 18 µJ-pulse to the 45 µJ-pulse leads to an increased free electron-density. This is not obtained for a time shift of $\Delta T \rightarrow \infty$ between the two pulses. Therefore, these experiments state that a previous pulse temporally increases the energy coupling between photons and electrons at least for 13.8 ns.

4. Conclusion

We perform time-resolved pump-probe reflectivity measurements to investigate the energy deposition of burst pulses in alkali aluminosilicate glass. These are complemented by ex situ topology analysis of the ablation width and depth. Temporal double pulses with single pulse energies of 18 µJ, 45 µJ and 72 µJ are utilized. The comparison between two configurations with $\Delta T = \rightarrow \infty$ and $\Delta T = 13.8$ ns exhibits two distinguishing features. First, the second pulse with $\Delta T = 13.8$ ns is shielded by the ablated material from

the previous pulse when it reaches the surface after the time of $\Delta T = 13.8\,\mathrm{ns}$. Second, the first pulse temporally lowers the threshold for photons to excite free electrons in glass in the irradiation zone for subsequent pulses. This feature was further investigated by lowering the pulse energy of the second pulse to the ablation threshold for single pulses. For the configuration with $\Delta T \to \infty$ no significant reflectivity increase is measured whereas the reflectivity of the pulse configuration with $\Delta T = 13.8\,\mathrm{ns}$ is increased. Therefore, the small temporal shift between the two pulses causes a higher relative reflectivity which is correlated to a higher free electron-density and a higher energy deposition.

Acknowledgements

This research was supported by the German Federal Ministry of Education and Research (BMBF) (Femto Digital Photonic Production 13N13307).

References

K. Mishchik, R. Beuton, O. Dematteo Caulier, S. Skupin, B. Chimier, G. Duchateau, B. Chassagne, R. Kling, C. Hönninger, E. Mottay, and J. Lopez, 2017. "Improved laser glass cutting by spatio-temporal control of energy deposition using bursts of femtosecond pulses," Opt. Express 25, 33271-33282

M. Kumkar, F. Zimmermann, J. Kleiner, D. Flamm, M. Jenne, D. Grossmann, S. Nolte, 2018. "Beam shaping and in-situ diagnostics for development of transparent materials processing," Proc. SPIE 10522, Frontiers in Ultrafast Optics: Biomedical, Scientific, and Industrial Applications XVIII, 105220H

M. Jenne, D. Flamm, T. Ouaj, J. Hellstern, J. Kleiner, D. Grossmann, M. Koschig, M. Kaiser, M. Kumkar, and S. Nolte, 2018. "High-quality tailored-edge cleaving using aberration-corrected Bessel-like beams," Opt. Lett. 43, 3164-3167

D. Flamm, D. G. Grossmann, M.l Jenne, F. Zimmermann, J. Kleiner, M. Kaiser, J. Hellstern, C. Tillkorn, M. Kumkar, 2019. "Beam shaping for ultrafast materials processing," Proc. SPIE 10904, Laser Resonators, Microresonators, and Beam Control XXI, 109041G

D. Grossmann, M. Reininghaus, C. Kalupka, M. Jenne, and M. Kumkar, 2017. "In-situ microscopy of front and rear side ablation processes in alkali aluminosilicate glass using ultra short pulsed laser radiation," Opt. Express 25, 28478-28488

M. Hermans, J. Gottmann, F. Riedel, 2014. "Selective, Laser-Induced Etching of Fused Silica at High Scan-Speeds Using KOH," Journal of Laser Micro / Nanoengineering 9

A. Vogel, J. Noack, G. Hüttmann, G. Paltauf, 2016. "Mechanisms of Femtosecond Laser Nanosurgery of Cells and Tissues, " Applied Physics B. 81

M. Sun, J. Zhu, Z. Lin, 2016. "Modeling of ablation threshold dependence on pulse duration for dielectrics with ultrashort pulsed laser," Opt. Eng. 56(1) 011026

C. Kalupka, D. Grossmann, M. Reininghaus, 2017. "Evolution of energy deposition during glass cutting with pulsed femtosecond laser radiation, " Applied Physics A. 123

D. Esser, S. Rezaei, J. Li, P. R. Herman, and J. Gottmann, 2011. "Time dynamics of burst-train filamentation assisted femtosecond laser machining in glasses," Opt. Express 19, 25632-25642

K. Bergner, M. Müller, R. Klas, J. Limpert, S. Nolte and A. Tünnerman, 2018. "Scaling ultrashort laser pulse induced glass modifications for cleaving applications," Appl. Opt. 57, 5941-5947

F. Hendricks, V. V. Matylitsky, M. Domke, H. P. Huber, 2016. "Time-resolved study of femtosecond laser induced micro-modifications inside transparent brittle materials," Proc. SPIE 9740, Frontiers in Ultrafast Optics: Biomedical, Scientific, and Industrial Applications XVI, 97401A

J. Hernandez-Rueda, D. Puerto, J. Siegel, M. Galvan-Sosa, J. Solis, 2012. "Plasma Dynamics and Structural Modifications Induced by Femtosecond Laser Pulses in Quartz, " Applied Surface Science. 258. 9389–9393

M. Garcia-Lechuga, J. Siegel, J. Hernandez-Rueda, J. Solis, 2014. "Femtosecond laser ablation of dielectric materials in the optical breakdown regime: Expansion of a transparent shell, " Applied Physics Letters. 105. 112902